Journal of Materials Chemistry A

PAPER

View Article Online
View Journal

Cite this: DOI: 10.1039/c4ta02052a

Flexible quantum dot-sensitized solar cells employing CoS nanorod arrays/graphite paper as effective counter electrodes

Miaoling Que,†[a] Wenxi Guo,†[a] Xiaojia Zhang,[a] Xiaoyi Li,[a] Qilin Hua,[a] Lin Dong*[ab] and Caofeng Pan*[a]

Received 25th April 2014
Accepted 16th June 2014

DOI: 10.1039/c4ta02052a

www.rsc.org/MaterialsA

We present a flexible solar cell which is composed of cobalt sulfide (CoS) nanorod arrays (NRAs) on graphite papers (GPs) (CoS NRAs/GP) as the counter electrode and CdS/CdSe quantum dot sensitized ZnO NRAs (CdS/CdSe@ZnO NRAs) as the photoanode. Orderly ZnO NRAs were directly fabricated on the flexible ITO/PET substrate by a hydrothermal method and CdS and CdSe quantum dots were subsequently deposited on them by chemical liquid deposition. CoS NRA/GP hybrid electrodes showed much higher electrocatalytic activity, higher exchange current density, and lower charge transfer resistance toward the reduction of S_x^{2-} ions compared to Pt and GP electrodes and they exhibited superior performance when functioning as counter electrodes (CEs) in CdS/CdSe quantum dot-sensitized solar cells (QDSSCs), 400–500% better than that with Pt and GP as counter electrodes. An absolute energy conversion efficiency of 2.70% has been demonstrated for the QDSSC employing an optimized CoS NRA/GP hybrid electrode, which was relatively higher than those of the QDSSCs featuring Pt (0.52%) and GP (0.71%) CEs. This work not only provides a hybrid electrode with high catalytic activity for QDSSCs, but also demonstrates a cost-effective way to fabricate flexible electrodes that can be applied in dye-sensitized solar cells or super capacitors.

1. Introduction

Along with the development of light-weight, miniaturization and high-integration electronic products, flexible and even folding electronic products increasingly become a hotspot for scientific research and manufacturing technology, which has broad prospects in defense electronic technology and healthcare.[1–5] The development of flexible electronic components largely depends on the development of the flexible, portable energy harvesting and energy storage systems. Miniaturized solar cells based on nanoarrays have been widely studied as the power supply for flexible microsystems and even nanosystems.[6,7] Quantum-dot sensitized solar cells (QDSSCs), as a promising type of new generation photovoltaic device, have received intensive attention due to their low cost, simple fabrication procedure and high theoretical power conversion efficiency.[8–14] In the fabrication of QDSSCs, high temperature annealing is widely used to obtain high-quality crystalline semiconductive electrodes, thus a major challenge preventing use of QDSSCs in flexible applications is the temperature limitation of plastic substrates.[15–17] An ideal solution for fabricating flexible semi-conductive electrodes is the direct growth of orderly one-dimensional and single-crystalline NRAs on these transparent and flexible plastic substrates without annealing.[18–24]

In addition, counter electrodes (CEs), as an important component in QDSSCs, play a crucial role in collecting electrons from the external circuit and reducing polysulfide (S^{2-}/S_x^{2-}) electrolytes. Because the sulfur atom present in polysulfide electrolytes can be easily adsorbed onto the surface of Pt CEs, metal sulfides including Cu_2S, CoS, PbS, and Cu_2S/reduced graphene oxide composites, *etc.* have been widely exploited.[25–29] However, most of the aforementioned studies are based on the powdered disordered metal sulfides and a method for effective growth of commonly used metal sulfide nanoarrays on the flexible substrates for QDSSCs is still an issue.[30]

Here, we present a flexible solar cell composed of a CoS NRA/GP hybrid counter electrode (CE) and a CdS/CdSe@ZnO NRA co-sensitized photoanode. The CoS NRA/GP hybrid CEs were prepared *via* a two-step solvothermal process using the aqueous solution. Compared to Pt and GP electrodes, CoS NRA/GP hybrid electrodes show much better electrocatalytic activity toward the reduction of S_x^{2-} ions. An absolute energy conversion efficiency of 2.70% has been demonstrated for the QDSSC employing an optimized CoS NRA/GP hybrid electrode. This work not only provides a hybrid electrode with high catalytic activity for QDSSCs, but also demonstrates a cost-effective way

[a]Beijing Institute of Nanoenergy and Nanosystems, Chinese Academy of Sciences, Beijing, 100083, P. R. China

[b]School of Materials Science and Engineering, Zhengzhou University, 450001, P. R. China. E-mail: cfpan@binn.cas.cn; donglin@binn.cas.cn

† Authors contributed equally to this work.

to fabricate metal sulfide NRAs on flexible substrates that can be applied in flexible devices for energy harvesting and storage.

2. Experimental section

2.1 Fabrication of CdS/CdSe@ZnO NRA photoanodes

ZnO NRAs were grown on the ITO/PET substrate by a hydrothermal method: a 50 nm thick ZnO seed layer was first sputtered on the ITO/PET substrate and then the substrate was fixed on a glass slide and put upside-down in a closed bottle with an aqueous solution comprising of zinc nitrate hexahydrate (50 mM) and hexamethylenetetramine (60 mM) at 85 °C for 8–12 h. Subsequently, CdS and CdSe QDs were deposited on the ZnO NRAs by chemical bath deposition (CBD) as previously reported by Zhang *et al.*[31] Firstly, ZnO NRAs were immersed in a solution of 0.1 M of Na_2S for 10 min at room temperature to form a thin ZnS layer on the surface of ZnO NRAs, which facilitated the deposition of CdS quantum dots. Then the sample was placed in a solution containing 0.025 M cadmium acetate, 0.1 M thiourea, and 0.1 M ethylenediamine for 1 h at room temperature to synthesize CdS/ZnO NRAs. Subsequently, the deposition of CdSe QDs was performed in 30 mL aqueous solution containing 0.015 g Se and 0.05 g $NaBH_4$ at 90 °C for 3 h, and this process was repeated twice. Finally, the obtained sample was rinsed with deionized water and dried in air.

2.2 Preparation of CEs

Followed by cleaning the GPs with ethanol and deionized water, respectively, the CoS NRAs were fabricated on the GPs by a two-step solvothermal process using the aqueous solution. First, a thin film of Co_3O_4 NRAs (~3 μm long) was grown on the GP substrate using chemical bath deposition (CBD) as previously reported by Kung *et al.*[32] The GP substrate was fixed on a glass slide and put upside-down in a closed bottle with an aqueous solution containing 1 M urea and 0.15 M $CoCl_2 \cdot 6H_2O$ at 90 °C for 2.5 h. Subsequently, the obtained Co_3O_4 NRAs were converted into CoS NRAs by soaking them in a closed bottle containing 0.01 M Na_2S aqueous solution at 120–160 °C for 8–16 h. Then, the obtained film was washed with deionized water and dried in air, thus obtaining the CoS NRA/GP CE.

2.3 Fabrication of QD sensitized solar cells

The CdSe/CdS@ZnO NRA photoanodes with an active area of approximately 0.126 cm^2 were packaged together with the above-prepared CEs by applying a 60 μm thick hot-melt sealed film as the spacer (SX1170-25; Solaronix Co.). A polysulfide electrolyte containing 0.5 M Na_2S, 0.2 M S, and 0.2 M KCl in a mixture of methanol and DIW (3 : 7 v/v) was injected into the space by a capillary effect.

2.4 Characterization

The morphology and structure of the prepared nanostructures of ZnO and CoS were examined by scanning electron microscopy (SEM-Hitachi 8000) and transmission electron microscopy (TEM-JEM 2100). The crystal structure information of CoS NRAs and precursor was obtained by X-ray diffraction (XRD) experiments on a PANalytical X'Pert PRO diffractometer. The light absorption of ZnO films with QDs was measured by UV-visible spectroscopy (Shimadzu UV-3600). Cyclic voltammetry (CV) measurements were performed with an Autolab electrochemical workstation, conventional three-electrode system and the CV curves were recorded at a scan rate of 50 mV s^{-1}, while the Tafel polarization curves were obtained using an Autolab electrochemical workstation at 5 mV s^{-1}, with a two-electrode system. One of the various CEs of QDSSCs, a platinum sheet, and a saturated calomel electrode (SCE) were used as the working electrode, CE, and reference electrode, respectively. The mixed solution of methanol and deionized water (3 : 7 v/v) containing 0.5 M Na_2S, 0.2 M S, and 0.2 M KCl was used as the electrolyte for all CV measurements. The two electrodes used in symmetrical cells were identical, being separated by a semi-permeable membrane, and the electrolyte used for the symmetrical cells was the same as that used for CV measurements. Electrochemical impedance spectra (EIS) were obtained in the frequency range of 100 kHz to 0.1 Hz and the corresponding AC amplitude of 10 mV using an Autolab model PGSTAT 30 (ECO Chemie B.V.) equipped with a Frequency Response Analyze (FRA) module (Autolab, Eco-Chemie), and the impedance spectra were analyzed using an equivalent circuit model. A Solux solar simulator was used to simulate sunlight for an illumination intensity of 100 mW cm^{-2} as calibrated with a Daystar meter. The solar cell was irradiated using a solar simulator (300 W model 91260, Newport) with an AM 1.5G spectrum distribution calibrated against an NREL reference cell to simulate accurately a full-sun intensity (100 mW cm^{-2}).

3. Results and discussion

Fig. 1a shows a schematic diagram of the flexible QDSSC, which is composed of CoS NRA/GP as the counter electrode, CdS/CdSe@ZnO NRAs as the flexible transparent top photoanode, and the polysulfide electrolyte is sandwiched by the parallel two electrodes. A cross-sectional view and the detailed structures of the QDSSC are shown in Fig. 1b. When sunlight irradiates

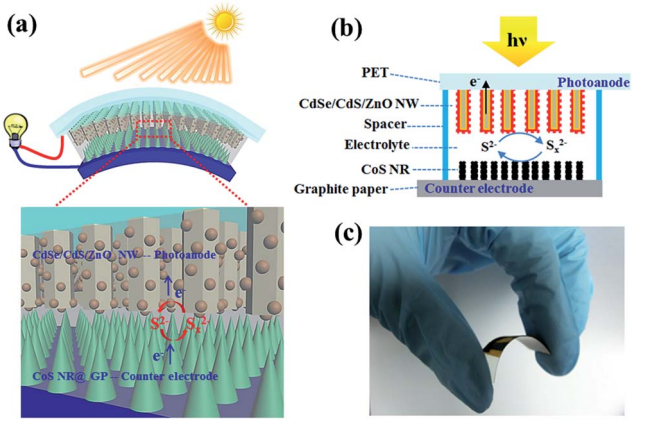

Fig. 1 (a) Structural schematic diagram of the flexible QDSSC. (b) Schematic illustration and working principle of the flexible QDSSC. (c) Digital photo of the flexible QDSSC.

through the CdS/CdSe@ZnO NRA photoanode, the excited electrons are rapidly injected into the conduction band of the ZnO NRAs and transported along the ITO/PET substrate, from which they flow to the CoS NRA/GP hybrid CE through an external circuit. The holes remaining at the sensitizer layer are captured by the reducing species in the polysulfide electrolyte, and the oxidized counter parts are reduced at the CE. A digital image of the fabricated QDSSC is shown in Fig. 1c, which shows excellent flexibility and sturdy construction of the device.

Fig. 2a and b show the scanning electron microscopy (SEM) images of ZnO NARs prepared on the ITO/PET substrate by hydrothermally reacting in 0.5 M zinc nitrate hexahydrate and 0.6 M hexamethylenetetramine at 85 °C for 10 h. It was observed that the as-fabricated ZnO NRAs had an average diameter and length of about 120 nm and 5 μm, respectively. After two-step chemical bath deposition (CBD), CdS and CdSe quantum dots (QDs) were deposited on the surface of ZnO NRAs and the SEM image is shown in Fig. 2c, which presents that the CdS and CdSe QDs were well-distinguished and uniformly distributed on the ZnO NRAs. Then the mass ratios of the co-sensitized film were further verified by the measurement of energy dispersive spectroscopy (EDS) shown in Fig. 2f, revealing that the prepared thin films are composed of Cd, Se, S, Zn and O. High-resolution transmission electron microscopy (HRTEM) measurement was performed to scrutinize the detailed structures of the as-fabricated CdSe/CdS@ZnO NRAs, as shown in Fig. 2d. It is clear that the sizes of QDs are in the range of 4–6 nm. The observed lattice spacing of 0.23 nm, 0.34 nm and 0.34 nm in the image corresponded to the (200), (111) and (111) planes of ZnO, CdS and CdSe, respectively. It is apparent, from the UV-vis light absorption spectra of ZnO NRAs and corresponding QD-sensitized ZnO NRAs shown in Fig. 2e, that CdS-sensitized NRA samples exhibited higher light absorption between 380 and 500 nm wavelength while the CdS and CdSe co-sensitized NRA samples exhibited higher light absorption in both UV and visible light regions. The inset in Fig. 2e shows the optical images of ZnO NRAs, CdS@ZnO NRAs and CdSe/CdS@ZnO NRAs (from left to right), respectively, indicating the changes in colour during the synthesis process.

As an intermediate, Co_3O_4 NRAs were firstly fabricated on the GP by the CBD method. As can be seen from the digital photograph in Fig. 3c, the grey black GP was covered by a red thin film after hydrothermal reaction in 1 M urea and 0.15 M $CoCl_2 \cdot 6H_2O$ at 90 °C for 2.5 h. Fig. 3a shows the corresponding SEM image of the red film on the GP, and it is clear that the entire surface of the GP was covered very uniformly by the NRAs that are dense and well-organized. A magnified SEM image of the NRAs is shown in the inset of Fig. 3a, which presents that the NRAs are needle-like, with diameters of 300–660 nm and lengths of 4.4–8.4 μm. The phase and purity of the as-obtained samples were examined by XRD shown in Fig. 3e. As revealed in

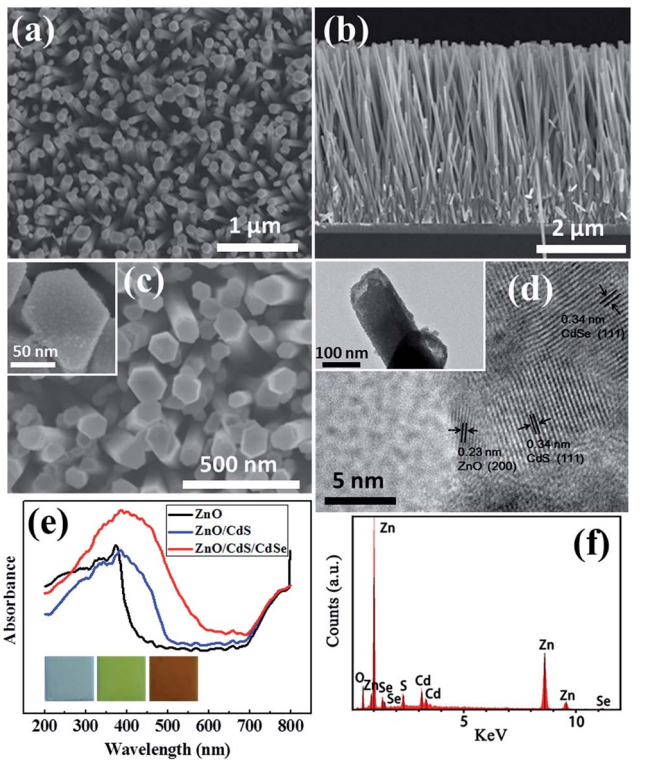

Fig. 2 (a) Top-view SEM image of ZnO NRAs grown on the PET substrate. (b) Cross-sectional SEM image of ZnO NRAs. (c) SEM image of CdS/CdSe@ZnO NRAs, the inset shows enlarged view of a CdS/CdSe@ZnO nanowire. (d) HRTEM image of a CdS/CdSe@ZnO nanorod, the inset shows the TEM image of CdS/CdSe@ZnO NRAs. (e) Light absorption spectra of as-prepared ZnO, CdS@ZnO, CdS/CdSe@ZnO NRAs, and the insets are their optical photos respectively (from left to right). (f) EDS spectra of a CdS/CdSe@ZnO NW.

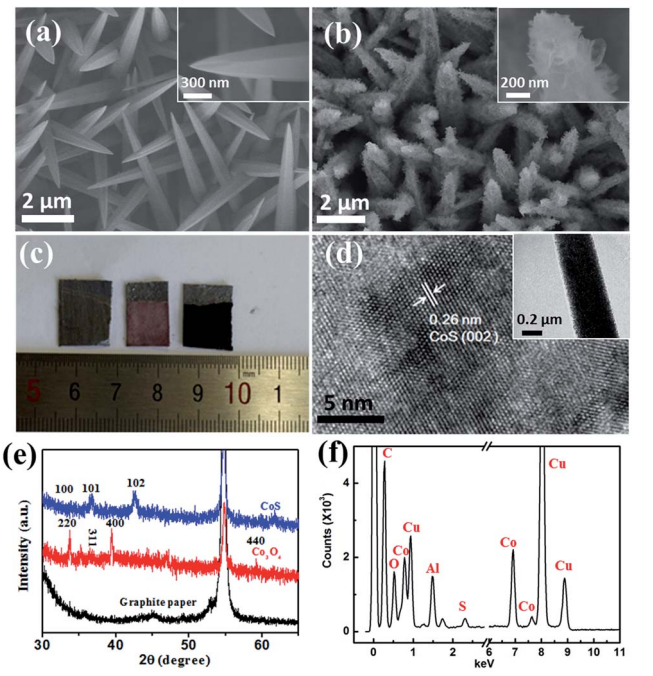

Fig. 3 SEM top-view images of (a) Co_3O_4 NRAs grown on the GP and (b) CoS NRAs grown on the GP. The insets in (a) and (b) are the corresponding enlarged views, respectively. (c) Digital photo of the graphite paper, Co_3O_4 NRA@GP and CoS NRA@GP (from left to right). (d) TEM and HRTEM image of a CoS nanorod. (e) XRD pattern of the CE samples. (f) EDS spectra of CoS NRAs grown on the GP.

patterns of GPs and Co_3O_4, all of the diffraction peaks of the red film can be indexed to Co_3O_4, according to Joint Committee on Powder Diffraction Standards (JCPDS card, file no. 80-1545).

The synthesized Co_3O_4 NRAs were used as templates and transformed into CoS NRAs in Na_2S aqueous solution. Obviously, the red film on GPs became black after 8 h hydrothermal treatment in Na_2S solution at 150 °C, as shown in Fig. 3c. The morphology of the as-prepared samples was examined by SEM in Fig. 3b. It is apparent that the needle-shaped heads disappeared and the surface of the NRAs became coarser after hydrothermal treatment. A SEM image (inset in Fig. 3b) with higher magnification shows that the arrays are porous and composed of numerous nanosheets. TEM and HRTEM were used to further examine the morphology and microstructure of the prepared NRAs. As can be seen from Fig. 3d, the HRTEM image of a NR, it can be observed that the interplanar spacing is 0.26 nm, corresponding to the separation between (002) lattice planes of CoS. The corresponding XRD pattern of CoS NRAs (Fig. 3e) reveals that the diffraction peaks of Co_3O_4 NRAs were disappeared and instead diffraction peaks were observed at $2\theta = 34.8°$, 36.1° and 42.5°, corresponding well to those of lattice planes (100), (101) and (102) for CoS (JCPDS card, file no. 75-0605). Subsequently, the mass ratios of the CoS film were further verified by the measurement of EDS shown in Fig. 3f, revealing that the prepared thin films are mainly composed of Co and S.

Fig. 4a shows the current density–voltage (J–V) characteristics of CdS/CdSe QD cosensitized ZnO NRA solar cells using CoS NRA/GP, GP and Pt as CEs under simulated AM 1.5G full sunlight intensity. An improved power conversion efficiency of 2.70% was achieved using CoS NRA@GP as the CE, yielding an open circuit voltage (V_{OC}) of 0.60 V, a short circuit current density (J_{SC}) of 12.6 mA cm^{-2}, and a fill factor (FF) of 0.36 which are shown in Table 1. It represents a superior PV characteristic especially in power conversion efficiency compared with devices employing GP and Pt CEs. The enhancement of power conversion efficiency is mainly attributed to the increase of J_{SC}, which reveals that reduction of the polysulfide redox species is faster at the CoS CE than GP and Pt CEs. The incident photon-to-current efficiency (IPCE) spectra as a function of wavelength were investigated to further evaluate the photovoltaic performance of the different CEs, which is shown in Fig. 4b. The IPCE value of CoS NRA/GP based QDSSCs in the wavelength region of 400–450 nm was nearly 90%, which was much higher than those of Pt and GP based QDSSCs. These results correlated well with the tendency of the value of J_{SC} observed from Table 1. What is more, in order to investigate the stability of the QDSSCs, a periodic bending test was performed by fixing the cells on the three-dimensional positioning system, as shown in the inset of Fig. 4c. The efficiency retentions in 500 bending cycles are presented in Fig. 4c, indicating that the flexible QDSSCs have remarkable mechanical robustness with minimal performance degradation even after 500 cycles of bending and relaxing.

To investigate the electrochemical catalytic activity of Pt, GP and CoS NRA@GP in the polysulfide electrolyte, cyclic voltammetry (CV) and Tafel polarization measurements were performed,[33,34] as shown in Fig. 5. During regeneration in the QDSSCs, the oxidized species, S_x^{2-}, had to be reduced to S^{2-} on

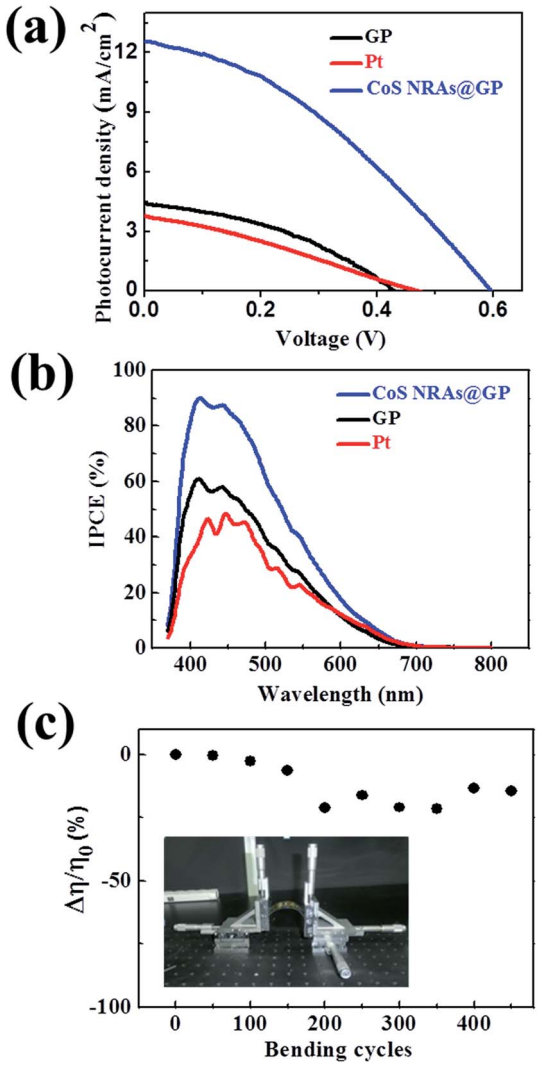

Fig. 4 (a) J–V characteristics of QDSSCs with GP, Pt, and Co_3O_4 NRA@GP as CEs, (b) IPCE spectra of QDSSCs with GP, Pt, and CoS NRA@GP as CEs, and (c) mechanical robust testing of the QDSSCs, where $\Delta\eta/\eta_0$ is the function of mechanical bending cycles, the inset shows the bending setups in the test.

the CE ($S_x^{2-} + 2e^- \leftrightarrow S_{x-1}^{2-} + S^{2-}$), therefore, the negative current in the CV plots can be used to evaluate the electrochemical catalytic activity toward the reduction of the polysulfide electrolyte. In this regard, the current densities at the reduction zone of CoS NRA/GP were conspicuously larger than those of GP and Pt electrodes, suggesting a higher catalytic activity for reducing S^{2-}/S_x^{2-} electrolytes. Subsequently, Tafel-polarization analysis was performed to further evaluate the electrocatalytic activity of the three kinds of CEs. The exchange current density (J_o) can be determined as the intercept of the extrapolated linear region of anodic and cathodic branches when the voltage is zero, and J_o also can be evaluated by the equation $J_o = RT/nFR_{ct}$, where R is the gas constant, T is the temperature, F is the Faraday constant and n is the number of electrons exchanged in the reaction at the electrolyte interface, that is to say, R_{ct} is inversely proportional to J_o, the lower R_{ct} and high J_o could provide a higher electrocatalytic activity of CEs.

Table 1 Electrochemical parameters for different CEs

CEs	R_s (Ω cm^2)	Y_0 (10^{-5} F cm^{-2} Sn^{-1})	n	R_{ct} (KΩ cm^2)	V_{OC} (V)	J_{SC} (mA cm^{-2})	FF	η (%)
Pt	44.8	21.7	0.8699	1574	0.47	3.28	0.29	0.52
GP	9.187	1104	0.4660	467.9	0.44	4.44	0.36	0.71
CoS NRA@GP	3.008	5615	0.4545	24.48	0.60	12.6	0.36	2.70

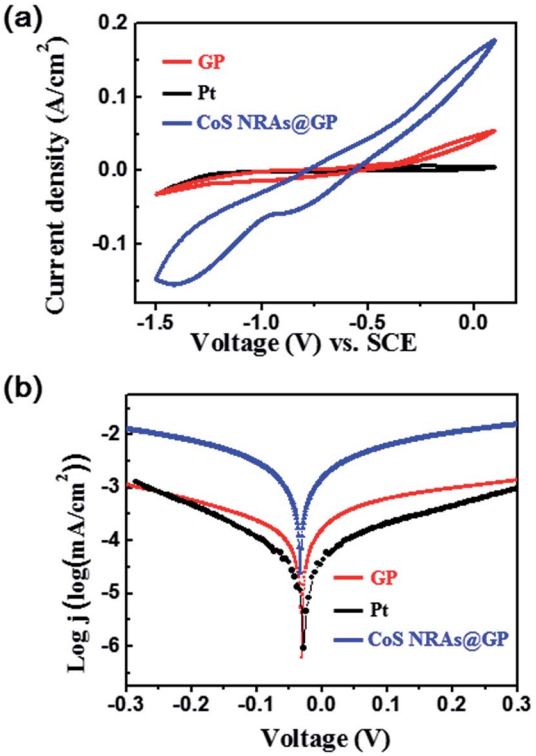

Fig. 5 (a) Cyclic voltammetry plots and (b) Tafel curves of GP, Pt, and Co_3O_4 NRA@GP three different CEs.

Fig. 5b represents that the CoS NRA/GP electrode has the highest J_o value and thus it has the best electrocatalytic activity, in good agreement with the tendency of R_{ct} observed from Table 1.

The electrochemical impedance spectra (EIS) measurements were also further performed to get more insight into the electrocatalytic kinetics of the CEs by measuring the charge-transfer resistance (R_{ct}), which is closely associated with the catalytic activity of the CEs.[32] Fig. 6 shows the Nyquist plots of the Pt, GP and CoS NRA/GP CEs; the equivalent circuit as shown in the top-left inset may be proposed to fit the Nyquist plots:[35,36] where R_s is the solution resistance, R_{ct} and Q_{dl} represent the charge transfer resistance and the double-layer capacitance of the electrode/electrolyte interface, respectively. The detailed EIS parameters are summarized in Table 1. The Nyquist plots demonstrated that the CoS NRA/GP electrode provided an apparent smaller R_{ct} value (24.48) than the other two CEs (1574 and 467.9), suggesting that the hybrid electrode could largely facilitate the electron transport from the CE to the S^{3-} species. Thus, cells employing CoS NRA/GP obtained a better photovoltaic performance than GP and Pt CEs.

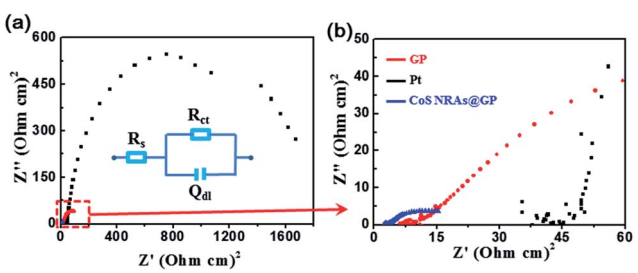

Fig. 6 Nyquist plots of QDSSCs with GP, Pt, and Co_3O_4 NRA@GP three different CEs. The inset depicts the expanded range of the low-value region and the corresponding equivalent circuit.

4. Conclusions

We have proposed an innovative and cost-effective approach to fabricate a kind of flexible QDSSC based on ZnO NRAs sensitized by CdS/CdSe QDs and CoS NRAs grown on the GP. CoS NRAs were successfully fabricated on the GP by reacting the Co_3O_4 NRAs with Na_2S aqueous solution. Compared with the traditional CEs of GP and Pt, the CoS NRA/GP electrode shows much higher electrocatalytic ability toward the reduction of S_x^{2-} ions. A power conversion efficiency of 2.70% is achieved for such QDSSCs with the CE of CoS NRA/GP. Combining the advantages of ZnO NRAs and CoS NRA/GP, this work not only developed a cost-effective way to fabricate flexible QDSSCs, but also opened up a new field in designing and fabricating high-performance catalysts by hybrid carbon materials and inorganic nanocrystals.

Acknowledgements

The authors thank for the support from the "thousands talents" program for pioneer researcher and his innovation team, China, the President Funding of the Chinese Academy of Sciences, the National Natural Science Foundation of China (no. 51272238 and 21321062), and the Innovation Talent Project of Henan Province (no. 13HASTIT020).

Notes and references

1 U. Bach, D. Lupo, P. Comte, J. E. Moser, F. Weissortel, J. Salbeck, H. Spreitzer and M. Gratzel, *Nature*, 1998, **395**, 583–585.

2 M. Z. Liu, M. B. Johnston and H. J. Snaith, *Nature*, 2013, **501**, 395–398.
3 B. Oregan and M. Gratzel, *Nature*, 1991, **353**, 737–740.
4 M. Durr, A. Schmid, M. Obermaier, S. Rosselli, A. Yasuda and G. Nelles, *Nat. Mater.*, 2005, **4**, 607–611.
5 D. H. Kim, J. H. Ahn, W. M. Choi, H. S. Kim, T. H. Kim, J. Z. Song, Y. G. Y. Huang, Z. J. Liu, C. Lu and J. A. Rogers, *Science*, 2008, **320**, 507–511.
6 C. F. Pan, W. X. Guo, L. Dong, G. Zhu and Z. L. Wang, *Adv. Mater.*, 2012, **24**, 3356–3361.
7 C. F. Pan, Z. X. Luo, C. Xu, J. Luo, R. R. Liang, G. Zhu, W. Z. Wu, W. X. Guo, X. X. Yan, J. Xu, Z. L. Wang and J. Zhu, *ACS Nano*, 2011, **5**, 6629–6636.
8 Y. Jiang, X. Zhang, Q. Q. Ge, B. B. Yu, Y. G. Zou, W. J. Jiang, W. G. Song, L. J. Wan and J. S. Hu, *Nano Lett.*, 2014, **14**, 365–372.
9 Z. S. Yang, C. Y. Chen, P. Roy and H. T. Chang, *Chem. Commun.*, 2011, **47**, 9561–9571.
10 S. Ruhle, M. Shalom and A. Zaban, *ChemPhysChem*, 2010, **11**, 2290–2304.
11 I. Mora-Sero, S. Gimenez, F. Fabregat-Santiago, R. Gomez, Q. Shen, T. Toyoda and J. Bisquert, *Acc. Chem. Res.*, 2009, **42**, 1848–1857.
12 H. Lee, M. K. Wang, P. Chen, D. R. Gamelin, S. M. Zakeeruddin, M. Gratzel and M. K. Nazeeruddin, *Nano Lett.*, 2009, **9**, 4221–4227.
13 P. V. Kamat, *J. Phys. Chem. C*, 2008, **112**, 18737–18753.
14 M. C. Hanna and A. J. Nozik, *J. Appl. Phys.*, 2006, **100**, 074510.
15 G. Hashmi, K. Miettunen, T. Peltola, J. Halme, I. Asghar, K. Aitola, M. Toivola and P. Lund, *Renewable Sustainable Energy Rev.*, 2011, **15**, 3717–3732.
16 D. C. Zou, D. Wang, Z. Z. Chu, Z. B. Lv and X. Fan, *Coord. Chem. Rev.*, 2010, **254**, 1169–1178.
17 M. Toivola, J. Halme, K. Miettunen, K. Aitola and P. D. Lund, *Int. J. Energy Res.*, 2009, **33**, 1145–1160.
18 M. Law, L. E. Greene, J. C. Johnson, R. Saykally and P. D. Yang, *Nat. Mater.*, 2005, **4**, 455–459.
19 S. Xu and Z. L. Wang, *Nano Res.*, 2011, **4**, 1013–1098.
20 W. X. Guo, C. Xu, X. Wang, S. H. Wang, C. F. Pan, C. J. Lin and Z. L. Wang, *J. Am. Chem. Soc.*, 2012, **134**, 4437–4441.
21 W. X. Guo, C. Xu, G. Zhu, C. F. Pan, C. J. Lin and Z. L. Wang, *Nano Energy*, 2012, **1**, 176–182.
22 W. X. Guo, F. Zhang, C. J. Lin and Z. L. Wang, *Adv. Mater.*, 2012, **24**, 4761–4764.
23 H. Q. Wang, L. C. Jia, P. Bogdanoff, S. Fiechter, H. Mohwald and D. Shchukin, *Energy Environ. Sci.*, 2013, **6**, 799–804.
24 H. Q. Wang, M. Miyauchi, Y. Ishikawa, A. Pyatenko, N. Koshizaki, Y. Li, L. Li, X. Y. Li, Y. Bando and D. Golberg, *J. Am. Chem. Soc.*, 2011, **133**, 19102–19109.
25 V. Gonzalez-Pedro, X. Q. Xu, I. Mora-Sero and J. Bisquert, *ACS Nano*, 2010, **4**, 5783–5790.
26 Z. Tachan, M. Shalom, I. Hod, S. Ruhle, S. Tirosh and A. Zaban, *J. Phys. Chem. C*, 2011, **115**, 6162–6166.
27 Z. S. Yang, C. Y. Chen, C. W. Liu, C. L. Li and H. T. Chang, *Adv. Energy Mater.*, 2011, **1**, 259–264.
28 X. Y. Yu, B. X. Lei, D. B. Kuang and C. Y. Su, *J. Mater. Chem.*, 2012, **22**, 12058–12063.
29 H. N. Chen, L. Q. Zhu, H. C. Liu and W. P. Li, *J. Phys. Chem. C*, 2013, **117**, 3739–3746.
30 H. W. Chen, C. W. Kung, C. M. Tseng, T. C. Wei, N. Sakai, S. Morita, M. Ikegami, T. Miyasaka and K. C. Ho, *J. Mater. Chem. A*, 2013, **1**, 13759–13768.
31 Z. Z. Lu, J. Xu, X. Xie, H. K. Wang, C. D. Wang, S. Y. Kwok, T. Wong, H. L. Kwong, I. Bello, C. S. Lee, S. T. Lee and W. J. Zhang, *J. Phys. Chem. C*, 2012, **116**, 2656–2661.
32 C. W. Kung, H. W. Chen, C. Y. Lin, K. C. Huang, R. Vittal and K. C. Ho, *ACS Nano*, 2012, **6**, 7016–7025.
33 P. Poudel, A. Thapa, H. Elbohy and Q. Qiao, *Nano Energy*, 2014, **5**, 116–121.
34 S. Sigdel, A. Dubey, H. Elbohy, A. Aboagye, D. Galipeau, L. Zhang, H. Fong and Q. Qiao, *J. Mater. Chem. A*, 2014, **2**, 11448–11453.
35 J. T. Zhang, J. M. Hu, J. Q. Zhang and C. N. Cao, *Prog. Org. Coat.*, 2004, **51**, 145–151.
36 C. Q. Ye, R. G. Hu, S. G. Dong, X. J. Zhang, R. Q. Hou, R. G. Du, C. J. Lin and J. S. Pan, *J. Electroanal. Chem.*, 2013, **688**, 275–281.

